Second-order nonlinear silicon-organic hybrid waveguides

L. Alloatti,[1,2,*] D. Korn,[1] C. Weimann,[1]C. Koos,[1,2] W. Freude,[1,2] and J. Leuthold[1,2]

[1] *Institute of Photonics and Quantum Electronics (IPQ), Karlsruhe Institute of Technology (KIT), 76131 Karlsruhe, Germany*

[2] *Institute of Microstructure Technology (IMT), Karlsruhe Institute of Technology (KIT), 76021 Karlsruhe, Germany*

[*]*luca.alloatti@kit.edu*

Abstract: We describe a concept for second-order nonlinear optical processes in silicon photonics. A silicon-organic hybrid (SOH) double slot waveguide is dispersion-engineered for mode phase-matching (MPM). The proposed waveguide enables highly efficient nonlinear processes in the mid-IR range. With a cladding nonlinearity of $\chi^{(2)} = 230$ pm/V and 20 dBm pump power at a CW wavelength of 1550 nm, we predict a gain of 14.7 dB/cm for a 3100 nm signal. The suggested structure enables for the first time efficient second-order nonlinear optical mixing in silicon photonics with standard technology.

References and links

1. R. W. Boyd, *Nonlinear Optics* (Academic Press, 2008).
2. M. Ebrahim-Zadeh and I. Sorokina, *Mid-Infrared Coherent Sources and Applications* (Springer, 2007).
3. A. Bogoni, X. X. Wu, Z. Bakhtiari, S. Nuccio, and A. E. Willner, "640 Gbits/s photonic logic gates," Opt. Lett. **35**(23), 3955–3957 (2010).
4. A. Galvanauskas, K. K. Wong, K. El Hadi, M. Hofer, M. E. Fermann, D. Harter, M. H. Chou, and M. M. Fejer, "Amplification in 1.2-1.7 μm communication window using OPA in PPLN waveguides," Electron. Lett. **35**(9), 731–733 (1999).
5. S. Barz, G. Cronenberg, A. Zeilinger, and P. Walther, "Heralded generation of entangled photon pairs," Nat. Photonics **4**(8), 553–556 (2010).
6. A. B. Sugiharto, C. M. Johnson, H. B. De Aguiar, L. Alloatti, and S. Roke, "Generation and application of high power femtosecond pulses in the vibrational fingerprint region," Appl. Phys. B-lasers and Optics **91**(2), 315–318 (2008).
7. S. V. Rao, K. Moutzouris, and M. Ebrahimzadeh, "Nonlinear frequency conversion in semiconductor optical waveguides using birefringent, modal and quasi-phase-matching techniques," J. Opt. A, Pure Appl. Opt. **6**(6), 569–584 (2004).
8. R. Soref, "Mid-infrared photonics in silicon and germanium," Nat. Photonics **4**(8), 495–497 (2010).
9. X. P. Liu, J. B. Driscoll, J. I. Dadap, R. M. Osgood, Jr., S. Assefa, Y. A. Vlasov, and W. M. J. Green, "Self-phase modulation and nonlinear loss in silicon nanophotonic wires near the mid-infrared two-photon absorption edge," Opt. Express **19**(8), 7778–7789 (2011).
10. A. Spott, Y. Liu, T. Baehr-Jones, R. Ilic, and M. Hochberg, "Silicon waveguides and ring resonators at 5.5 mu m," Appl. Phys. Lett. **97**(21), 213501 (2010).
11. F. X. Li, S. D. Jackson, C. Grillet, E. Magi, D. Hudson, S. J. Madden, Y. Moghe, C. O'Brien, A. Read, S. G. Duvall, P. Atanackovic, B. J. Eggleton, and D. J. Moss, "Low propagation loss silicon-on-sapphire waveguides for the mid-infrared," Opt. Express **19**(16), 15212–15220 (2011).
12. S. Zlatanovic, J. S. Park, S. Moro, J. M. C. Boggio, I. B. Divliansky, N. Alic, S. Mookherjea, and S. Radic, "Mid-infrared wavelength conversion in silicon waveguides using ultracompact telecom-band-derived pump source," Nat. Photonics **4**(8), 561–564 (2010).
13. R. Shankar, R. Leijssen, I. Bulu, and M. Lončar, "Mid-infrared photonic crystal cavities in silicon," Opt. Express **19**(6), 5579–5586 (2011).
14. V. Raghunathan, D. Borlaug, R. R. Rice, and B. Jalali, "Demonstration of a mid-infrared silicon Raman amplifier," Opt. Express **15**(22), 14355–14362 (2007).
15. M. M. Milosevic, P. S. Matavulj, P. Y. Y. Yang, A. Bagolini, and G. Z. Mashanovich, "Rib waveguides for mid-infrared silicon photonics," JOSA B **26**, 1760–1766 (2009).

16. R. S. Jacobsen, K. N. Andersen, P. I. Borel, J. Fage-Pedersen, L. H. Frandsen, O. Hansen, M. Kristensen, A. V. Lavrinenko, G. Moulin, H. Ou, C. Peucheret, B. Zsigri, and A. Bjarklev, "Strained silicon as a new electro-optic material," Nature **441**(7090), 199–202 (2006).
17. M. A. Foster, A. C. Turner, J. E. Sharping, B. S. Schmidt, M. Lipson, and A. L. Gaeta, "Broad-band optical parametric gain on a silicon photonic chip," Nature **441**(7096), 960–963 (2006).
18. B. Kuyken, H. Ji, S. Clemmen, S. K. Selvaraja, H. Hu, M. Pu, M. Galili, P. Jeppesen, G. Morthier, S. Massar, L. K. Oxenløwe, G. Roelkens, and R. Baets, "Nonlinear properties of and nonlinear processing in hydrogenated amorphous silicon waveguides," Opt. Express **19**(26), B146–B153 (2011).
19. M. Cazzanelli, F. Bianco, E. Borga, G. Pucker, M. Ghulinyan, E. Degoli, E. Luppi, V. Véniard, S. Ossicini, D. Modotto, S. Wabnitz, R. Pierobon, and L. Pavesi, "Second-harmonic generation in silicon waveguides strained by silicon nitride," Nat. Mater. **11**(2), 148–154 (2011).
20. N. K. Hon, K. K. Tsia, D. R. Solli, and B. Jalali, "Periodically poled silicon," Appl. Phys. Lett. **94**(9), 091116 (2009).
21. I. Avrutsky and R. Soref, "Phase-matched sum frequency generation in strained silicon waveguides using their second-order nonlinear optical susceptibility," Opt. Express **19**(22), 21707–21716 (2011).
22. B. Chmielak, M. Waldow, C. Matheisen, C. Ripperda, J. Bolten, T. Wahlbrink, M. Nagel, F. Merget, and H. Kurz, "Pockels effect based fully integrated, strained silicon electro-optic modulator," Opt. Express **19**(18), 17212–17219 (2011).
23. T. W. Baehr-Jones and M. J. Hochberg, "Polymer silicon hybrid systems: A platform for practical nonlinear optics," J. Phys. Chem. C **112**(21), 8085–8090 (2008).
24. J. Leuthold, W. Freude, J. M. Brosi, R. Baets, P. Dumon, I. Biaggio, M. L. Scimeca, F. Diederich, B. Frank, and C. Koos, "Silicon organic hybrid technology-A platform for practical nonlinear optics," Proc. IEEE **97**(7), 1304–1316 (2009).
25. M. Jazbinsek, L. Mutter, and P. Gunter, "Photonic applications with the organic nonlinear optical crystal DAST," IEEE J. Sel. Top. Quantum Electron. **14**(5), 1298–1311 (2008).
26. Y. Enami, C. T. Derose, D. Mathine, C. Loychik, C. Greenlee, R. A. Norwood, T. D. Kim, J. Luo, Y. Tian, A. K. Y. Jen, and N. Peyghambarian, "Hybrid polymer/sol-gel waveguide modulators with exceptionally large electro-optic coefficients," Nat. Photonics **1**(3), 180–185 (2007).
27. GigOptix, *www.gigoptix.com.*
28. L. Alloatti, D. Korn, R. Palmer, D. Hillerkuss, J. Li, A. Barklund, R. Dinu, J. Wieland, M. Fournier, J. Fedeli, H. Yu, W. Bogaerts, P. Dumon, R. Baets, C. Koos, W. Freude, and J. Leuthold, "42.7 Gbit/s electro-optic modulator in silicon technology," Opt. Express **19**(12), 11841–11851 (2011).
29. M. Zhu, H. Liu, X. Li, N. Huang, Q. Sun, J. Wen, and Z. Wang, "Ultrabroadband flat dispersion tailoring of dual-slot silicon waveguides," Opt. Express **20**(14), 15899–15907 (2012).
30. C. M. Herzinger, B. Johs, W. A. McGahan, J. A. Woollam, and W. Paulson, "Ellipsometric determination of optical constants for silicon and thermally grown silicon dioxide via a multi-sample, multi-wavelength, multi-angle investigation," J. Appl. Phys. **83**(6), 3323–3336 (1998).
31. E. D. Palik, *Handbook of optical constants of solids* (Academic Press, 1997).
32. E. Jordana, J. M. Fedeli, P. Lyan, J. P. Colonna, P. Gautier, N. Daldosso, L. Pavesi, Y. Lebour, P. Pellegrino, B. Garrido, J. Blasco, F. Cuesta-Soto, and P. Sanchis, "Deep-UV lithography fabrication of slot waveguides and sandwiched waveguides for nonlinear applications," 2007 4th IEEE Int. Conf. Group IV Photon., 217–219 (2007).
33. C. Vassallo, *Optical Waveguide Concepts* (Elsevier, 1991).
34. R. Dinu, Dan Jin, Guomin Yu, Baoquan Chen, Diyun Huang, Hui Chen, A. Barklund, E. Miller, C. Wei, and J. Vemagiri, "Environmental stress testing of electro-optic polymer modulators," J. Lightwave Technol. **27**(11), 1527–1532 (2009).
35. A. D. Bristow, N. Rotenberg, and H. M. van Driel, "Two-photon absorption and Kerr coefficients of silicon for 850-2200 nm," Appl. Phys. Lett. **90**(19), 191104 (2007).
36. L. R. Dalton, S. J. Benight, L. E. Johnson, D. B. Knorr, Jr., I. Kosilkin, B. E. Eichinger, B. H. Robinson, A. K. Y. Jen, and R. M. Overney, "Systematic nanoengineering of soft matter organic electro-optic materials," Chem. Mater. **23**(3), 430–445 (2011).
37. C. Koos, P. Vorreau, T. Vallaitis, P. Dumon, W. Bogaerts, R. Baets, B. Esembeson, I. Biaggio, T. Michinobu, F. Diederich, W. Freude, and J. Leuthold, "All-optical high-speed signal processing with silicon-organic hybrid slot waveguides," Nat. Photonics **3**(4), 216–219 (2009).
38. Q. Lin, O. J. Painter, and G. P. Agrawal, "Nonlinear optical phenomena in silicon waveguides: Modeling and applications," Opt. Express **15**(25), 16604–16644 (2007).
39. T. Vallaitis, S. Bogatscher, L. Alloatti, P. Dumon, R. Baets, M. L. Scimeca, I. Biaggio, F. Diederich, C. Koos, W. Freude, and J. Leuthold, "Optical properties of highly nonlinear silicon-organic hybrid (SOH) waveguide geometries," Opt. Express **17**(20), 17357–17368 (2009).
40. R. Kitamura, L. Pilon, and M. Jonasz, "Optical constants of silica glass from extreme ultraviolet to far infrared at near room temperature," Appl. Opt. **46**(33), 8118–8133 (2007).
41. C. G. Poulton, C. Koos, M. Fujii, A. Pfrang, T. Schimmel, J. Leuthold, and W. Freude, "Radiation modes and roughness loss in high index-contrast waveguides," IEEE J. Sel. Top. Quantum Electron. **12**(6), 1306–1321 (2006).

42. R. Ding, T. Baehr-Jones, W. J. Kim, X. G. Xiong, R. Bojko, J. M. Fedeli, M. Fournier, and M. Hochberg, "Low-loss strip-loaded slot waveguides in Silicon-on-Insulator," Opt. Express **18**(24), 25061–25067 (2010).
43. R. Sun, P. Dong, N. N. Feng, C. Y. Hong, J. Michel, M. Lipson, and L. Kimerling, "Horizontal single and multiple slot waveguides: optical transmission at lambda = 1550 nm," Opt. Express **15**(26), 17967–17972 (2007).
44. J. Leuthold, J. Eckner, E. Gamper, P. A. Besse, and H. Melchior, "Multimode interference couplers for the conversion and combining of zero- and first-order modes," J. Lightwave Technol. **16**(7), 1228–1239 (1998).
45. B. Esembeson, M. L. Scimeca, T. Michinobu, F. Diederich, and I. Biaggio, "A high-optical quality supramolecular Assembly for third-order integrated nonlinear optics," Adv. Mater. (Deerfield Beach Fla.) **20**(23), 4584–4587 (2008).
46. C. Koos, L. Jacome, C. Poulton, J. Leuthold, and W. Freude, "Nonlinear silicon-on-insulator waveguides for all-optical signal processing," Opt. Express **15**(10), 5976–5990 (2007).

1. Introduction

Second-order nonlinear processes, like sum- and difference-frequency generation, spontaneous down-conversion and optical parametric amplification [1], are essential for a number of applications, ranging from spectroscopy, free-space communication, biochemical sensing, medical therapy [2], ultra-fast optical signal processing [3], lowest-noise optical amplification [4], and quantum physics [5]. Since at least one of the frequencies involved in a three-wave mixing process is necessarily well separated from the others, second-order processes represent additionally an excellent candidate for generating mid-IR and far-IR wavelengths [6].

Efficient nonlinear conversions require materials with strong nonlinearities, high-optical intensities and phase-matching between the waves involved [1]. So far, second-order nonlinear waveguides have been made of polymers, GaAs, InP, and LiNbO$_3$ [7], and phase-matching has successfully been achieved by birefringence, intermodal dispersion, or quasi-phase-matching. These materials often require specialized process technologies which are not applicable for mass production. Further, the relatively small index contrasts which can be achieved limit the modal confinement in waveguides. Conversion efficiencies are hence small and optical output powers in the µW range are considered high [7].

Silicon photonics, on the other hand, is based on a widely available technology, and allows fabricating high-index contrast waveguides for obtaining the required intensities with low optical powers. The vision of creating mid-IR applications using the inexpensive silicon-photonics platform [8] has already led to a number of publications in the following topics: Silicon waveguides pumped below the two-photon absorption (TPA) edge with powers as high as 33.5 W (45 dBm) [9], low-loss propagation in the 2-6 µm wavelength range [10, 11], light generation at 2.4 µm with standard telecom sources [12], high-Q SOI photonic crystal cavities at 4.4 µm [13], Raman amplification at 3.39 µm [14], and extensive simulations for single-mode operation and polarization-independent operation in SOI rib waveguides in the mid-IR region [15].

However, unstrained crystalline silicon is centro-symmetric, and its second-order nonlinearity is vanishing [16]. As a consequence, mid-IR generation in unstrained silicon waveguides has to rely on the third-order nonlinearity [9], taking advantage of the "built-in" strong Kerr nonlinearity of crystalline [17] or amorphous silicon [18]. This, in turn, results in high pump power requirements.
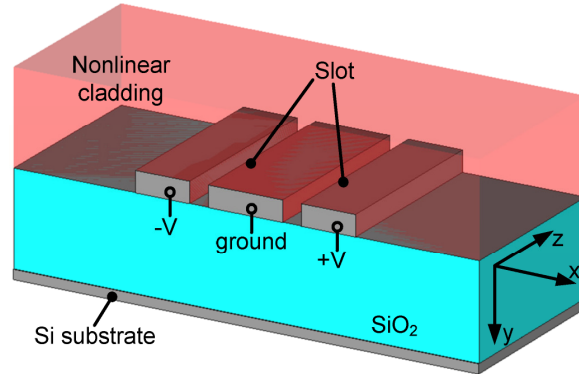
Fig. 1. Silicon organic-hybrid (SOH) double slot waveguide for second-order nonlinear applications. The waveguide consists of three silicon strips on a glass substrate, it is multimode and dimensioned such that modal phase-matching is achieved. The waveguide is covered by a nonlinear cladding, which is poled during fabrication by applying the voltages – V and + V to the outermost strips while the central strip is grounded. As a result the nonlinear second-order susceptibility is high only inside the slots.

In silicon photonics, first attempts of second-harmonic generation are based on strained waveguides, but despite nanosecond peak pump powers as high as 0.7 W, the output peak powers are limited to only 40 nW [19]. The small efficiency is due to a non-phase-matched design. A method for achieving quasi-phase-matching (QPM) in periodically strained silicon has already been proposed [20], however large mode sizes and small nonlinearities lead to normalized conversion efficiencies smaller than 1% $W^{-1}cm^{-2}$. More recently, a method of achieving phase-matching based on birefringence in strained silicon waveguides has been proposed [21], but the efficiency of the device relies on nonlinearities which have not been shown so far in waveguides of the proposed size [22]. Finally, the potential high efficiencies of SOH second-order nonlinear waveguides have already been discussed [23], but unfortunately no waveguide design has been proposed so far.

In this paper we propose for the first time a second-order nonlinear silicon-organic hybrid (SOH) waveguide [24] based on standard silicon-on-insulator (SOI) technology. The device is suited for efficient mid-IR generation and amplification, Fig. 1. We predict optical pump powers that are orders of magnitude smaller than for Kerr-nonlinear devices. The nonlinearity is provided by a specially engineered nonlinear organic cladding [25, 26], and a novel double slot geometry enables both strong interaction with the nonlinear material and phase-matching. We confirm the viability of our concept by extensive numerical simulations and give design guidelines for covering a broad wavelength range.

This paper is structured as follows: In Section 2 we describe the structure of the proposed device. In Section 3 the phase-matching condition is investigated in detail. In Section 4 the conversion efficiency is calculated and the required optical powers are discussed. In Appendix A, we present a mode-converter for exciting the required modes. In Appendix B we compare the optical electric field strengths needed for generating a given nonlinear polarization. We show that the required pump field is orders of magnitude smaller for second-order than for third-order nonlinearities.
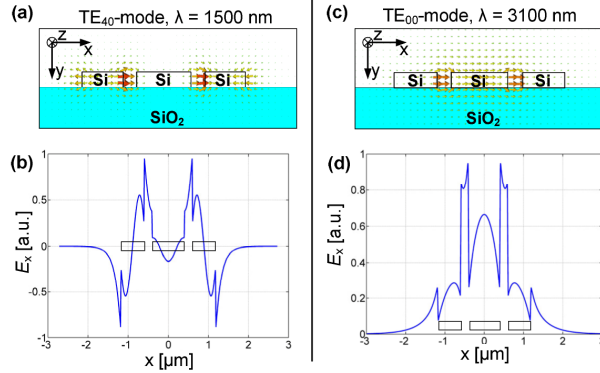
Fig. 2. Transverse electric fields for pump mode and signal/idler mode. (a) Quasi-TE$_{40}$ pump mode at λ = 1500 nm. Light is strongly confined to the two slots where the nonlinear interaction takes place. (b) Dominant horizontal electric field component E_x of TE$_{40}$ mode at half the strip waveguide height. (c) Fundamental quasi-TE$_{00}$ mode at λ = 3100 nm for signal and idler. Also in this case, light is strongly confined to the two slots. (d) Dominant horizontal electric field component E_x of the fundamental TE$_{00}$ mode at half the strip waveguide height.

2. The device concept

A sketch of the proposed second-order nonlinear device is displayed in Fig. 1. It consists of three parallel silicon strips (double slot waveguide) realized on a standard silicon-on-insulator (SOI) wafer having an oxide thickness of 2 μm and a device layer of 220 nm. The waveguide is spin coated with polymer-dispersed nonlinear chromophores [27], which have a high $\chi^{(2)}$-nonlinearity only inside the two slots. This can be experimentally achieved by poling [28] the material at its glass transition temperature, and by applying two voltages as shown in Fig. 1.

For definitiveness, we will describe a device for difference-frequency generation (DFG) with a pump wavelength of 1.5 μm, a signal wavelength of 2.9 μm and an idler wavelength close to 3.1 μm. Signal and idler propagate in a mode different from the mode in which the pump light is guided. The concept, however, is more general and may be applied to other spectral ranges as will be outlined below.

The waveguide is dimensioned such that modal phase-matching (MPM) is achieved [7] between the quasi-TE$_{40}$ mode for the pump (four nodes in the horizontal direction, zero nodes in the vertical direction) and the fundamental quasi-TE$_{00}$ mode for signal and idler; the corresponding mode profiles are shown in Fig. 2. These modes can be excited efficiently with mode converters described in Appendix A. We did not find any combination of (the first six) modes which could satisfy MPM in waveguides with a single slot, and the solution presented here is the one with the lowest mode-order that we could find in double slot waveguides. Finally, it is worth noticing that dispersion engineering in double slot waveguides has already been exploited in the context of third-order nonlinear processes [29].

3. Phase-matching

The frequencies at which MPM is achieved depend on the dispersion of the (quasi-)TE$_{00}$ and the (quasi-)TE$_{40}$ modes. As an example, we will now consider a waveguide dimensioned as follows: Width of the outermost strips 580 nm, slot width 200 nm, width of the central strip 800 nm; these values are well within the capabilities of current silicon-photonic foundries. The dispersion diagram of the TE$_{00}$ and the TE$_{40}$ modes is shown in the frequency range from 50 THz to 250 THz (wavelength range from 6 μm to 1.2 μm), Fig. 3 (a). Material dispersion for modeling the refractive index of the thermal oxide beneath the

silicon waveguide is taken from [30], while the corresponding data for crystalline silicon are from [31]. The corresponding curves are also shown in Fig. 3(a).
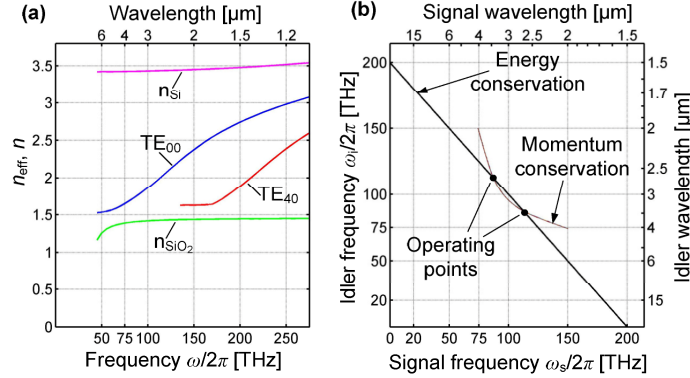

Fig. 3. Mode dispersion and phase-matching conditions for a typical waveguide. (a) Effective index n_{eff} for TE_{00} and TE_{40} TE-modes are plotted vs. frequency (bottom axis) or wavelength (top axis). The refractive indices of silicon and of silicon dioxide used in the simulation are also plotted. (b) Signal and idler frequencies for energy and momentum conservation. The straight line describes energy conservation while he curved line represents the condition for momentum conservation according to Eq. (1). Geometry considered in this example: Side-strip/slot/central-strip widths are 580/200/800 nm. In order to take into account the material dispersion of the nonlinear polymer cladding, a refractive index of 1.58 was assumed for calculating the signal and idler mode, while a refractive index of 1.68 was assumed for the pump mode.

In Fig. 3(b) we analyze the conditions for MPM, based on the data of Fig. 3(a). The straight black line represents the dependence of idler frequency on signal frequency which have to sum up to the pump frequency (in this example 200 THz, energy conservation), and the curved line represents the points where phase-matching is achieved (momentum conservation) [1],

$$\hbar\omega_s + \hbar\omega_i = \hbar\omega_p,$$
$$\hbar k_s + \hbar k_i = \hbar k_p, \qquad k_{p,s,i,} = n_{\mathrm{eff},p,s,i}\,\omega_{p,s,i}\,/c, \qquad (1)$$

where c is the speed of light, k is the wavevector component along the waveguide direction, ω is the angular frequency and s, i, p stand for signal, idler and pump respectively. The intersections of the two curves determine the operating points of the device, i. e., they fix signal and idler frequencies.

As can be seen from Fig. 3(b), a pump frequency of 200 THz yields operating points with signal and idler frequencies at about 115 THz and 85 THz.

Choosing a different pump frequency will result in other operating points that strongly depend on the particular dispersion of the waveguide. This information is represented in Fig. 4. The three curves stand for three different waveguide geometries which can be chosen by the user according to the desired pump and signal wavelengths. The cyan regions show the frequencies for which the coherent buildup length $L_{\mathrm{coh}} = 2 / (k_s + k_i - k_p)$ [1] is equal or larger than 1 cm. A wavelength detuning of 50 nm or more from the ideal therefore still allows a coherent buildup of the converted wave, showing that the wavelength tuning requirements are very relaxed. From Fig. 4 it can also be deduced that the required fabrication tolerances are in the 10 nm range, i. e. within the capabilities of today's silicon photonics foundries. Additionally, the strip and slot size are relatively large [28], meaning that the waveguide can be fabricated by means of standard 193 nm DUV lithography [32]. The full fabrication of the

device consists therefore in creating the passive structures in a CMOS fab followed by a post-processing spin coating and poling of the nonlinear material.
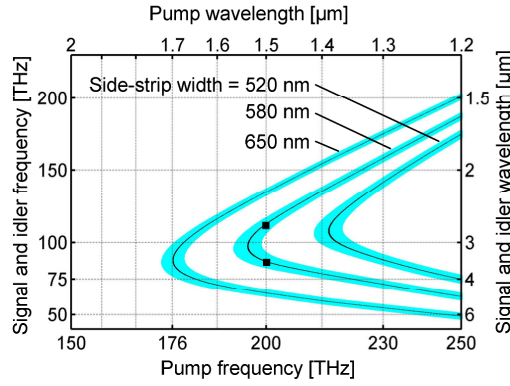

Fig. 4. Signal and idler frequencies vs. pump frequency for three different geometries. The black curves specify for a given pump frequency the signal and idler frequencies which satisfy the energy conservation and the phase-matching condition Eq. (1). The cyan-colored regions indicate the frequency space where the coherent buildup length $L_{coh} = 2 / (k_s + k_i - \square k_p)$ [1] is equal to 1 cm or longer. The three different curves represent waveguides where the side-strip width is set to 520 nm, 580 nm and 650 nm. The central-strip width is 800 nm and the slot width is 200 nm in all the three cases. For a side-strip width of e.g. 580 nm and a pump wavelength of 1.5 µm (200 THz), signal and idler wavelengths of 2.6 µm and 3.5 µm would result (square symbols).

4. Power levels and conversion efficiencies

In this section we analyze numerically the performance of the proposed waveguide and show that small optical power levels can lead to significant optical output power or optical gain. To this end, we consider here again the case of difference-frequency generation (DFG); a similar analysis can be applied to any other three-wave mixing process.

We define the nth complex electric field component ($n = 1, 2, 3$) in a Cartesian coordinate (x, y, z)- system by separating a dimensionless amplitude $A(\omega)$ from the modal field $\mathcal{E}_n^+(\omega, x, y)$. A propagator describes the wave propagation of a monochromatic wave with angular frequency ω and propagation constant k along the z-direction,

$$E_n(x, y, z, t) = A(\omega, z)\mathcal{E}_n^+(\omega, x, y)\,\mathrm{e}^{\mathrm{i}(kz - \omega t)} + \mathrm{cc}. \qquad (2)$$

In Eq. (2), cc stands for the complex conjugate of the foregoing expression, and the mode normalization is chosen such that the time-averaged power transported by the electromagnetic wave in Eq. (2) is equal to 1 mW when the dimensionless coefficient $A(\omega)$ is equal to one.

In the slowly-varying amplitude approximation it can be shown [1, 33] that the idler and signal amplitudes satisfy the following coupled differential equations (propagation loss as well as pump depletion are neglected, $A(\omega_p, z) = $ const; spatial dependency omitted)

$$\frac{\partial A(\omega_i)}{\partial z} = \mathrm{i}\gamma_i A(\omega_p)A^*(\omega_s) \qquad (3)$$

$$\frac{\partial A(\omega_s)}{\partial z} = \mathrm{i}\gamma_s A(\omega_p)A^*(\omega_i), \qquad (4)$$

where we find for the second-order field interaction factor (using Einstein's summation convention and dropping the spatial coordinates for simplicity)

$$\gamma_i = \frac{\epsilon_0 \omega_i}{\int \mathrm{d}x\mathrm{d}y \left[\mathcal{E}^+(\omega_i) \times \mathcal{H}^+(\omega_i) \right]_z} \int \mathrm{d}x\mathrm{d}y \ \chi_{lmn}^{(2)} \left[\mathcal{E}_l^-(\omega_i) \right]^* \left[\mathcal{E}_m^+(\omega_s) \right]^* \mathcal{E}_n^+(\omega_p) \quad (5)$$

$$\gamma_s = \frac{\epsilon_0 \omega_s}{\int \mathrm{d}x\mathrm{d}y \left[\mathcal{E}^+(\omega_s) \times \mathcal{H}^+(\omega_s) \right]_z} \int \mathrm{d}x\mathrm{d}y \ \chi_{lmn}^{(2)} \left[\mathcal{E}_l^-(\omega_s) \right]^* \left[\mathcal{E}_m^+(\omega_i) \right]^* \mathcal{E}_n^+(\omega_p), \quad (6)$$

where $\mathcal{E}_i^{+(-)}$ represents a forward (back) propagating mode.

The solution of the coupled Eqs. (5) and (6) for the case of zero idler at $z = 0$, $A(\omega_i, z = 0) = 0$, is given by

$$A(\omega_s, z) = A(\omega_s, z = 0)\cos h(\kappa z) \to \tfrac{1}{2}A(\omega_s, z = 0)e^{\kappa z} \ \text{ for } z \to \infty \quad (7)$$

$$A(\omega_i, z) = \mathrm{i}\sqrt{\frac{\gamma_i}{\gamma_s}} \frac{A(\omega_p)}{|A(\omega_p)|} A^*(\omega_s, z = 0)\sin h(\kappa z) \quad (8)$$

where

$$\kappa = |A(\omega_p)| (\gamma_s \gamma_i)^{1/2} \quad (9)$$

determines the optical (amplitude) gain. A convenient and common quantity [7] for representing the device performance is the normalized conversion efficiency, which is defined by

$$\eta = \lim_{z \to 0} P_i(z) / \left(P_s(0)P_p(0)z^2 \right) = \gamma_s \gamma_i \ /\mathrm{mW} \ , \quad (10)$$

where $P_{i,s,p}(z)$ is the power of the different lightwaves at position z.

For the sake of illustration, we now estimate the nonlinear susceptibility for the organic material M1 which we already used in SOH modulators [28]. This material consists of chromophores dispersed in a polymer matrix, is commercially available at GigOptix [27, 28] and shows an electro-optic coefficient of $r_{33} = 70$ pm/V at the wavelength of 1550 nm. Nonlinear polymers can efficiently be poled in silicon slot waveguides [28] and have reached very high stability, as it has been recently certified by Telcordia [34]. Unfortunately however, for the frequencies involved, no data are available for the nonlinear susceptibility $\chi_{lmn}(\omega_i; \omega_s, \omega_p)$ of the material M1. We adopt therefore the approximation $|\chi_{lmn}| = \delta_{1l}\delta_{1m}\delta_{1n} \ n^4 \ |r_{lmn}|/2$ [25], which leads for $n = 1.6$ to $|\chi_{111}| = 230$ pm/V. Assuming further that the nonlinear susceptibility is non-zero only inside the slot, we evaluate numerically the integrals Eq. (5), (6) for the geometry considered in Fig. 3, and find

$$\gamma_s \approx \gamma_i \approx 16.9 \ \mathrm{m}^{-1}, \quad (11)$$

which correspond to an impressive normalized conversion efficiency

$$\eta = 29 \ \mathrm{W}^{-1}\mathrm{cm}^{-2} \quad \left(2900 \% \ \mathrm{W}^{-1}\mathrm{cm}^{-2} \right). \quad (12)$$

As an example, assuming a CW pump power of 20 dBm, i.e. $A(\omega_p) = 10$, Eq. (7) and (11) lead to $\kappa = 1.69$ cm^{-1}, which corresponds to a power gain equal to 14.7 dB/cm in the limit of long device length. As a second example, assuming 20 dBm CW input pump power, -10 dBm signal input power, no idler at the input and neglecting losses, Eq. (8) implies that after propagating through a 1 cm long waveguide the idler has a power of 0.68 mW (-1.7 dBm), and the signal has a power of 0.78 mW (-1.1 dBm).

We observe that the assumed nonlinear susceptibility of 230 pm/V is a very conservative value. In fact, nonlinear susceptibilities of 354 pm/V have already been measured at optical

frequencies in nonlinear polymers [35], and this value increases to 580 pm/V for organic crystals [25]. Moreover, $\chi^{(2)}$ values up to 830 pm/V have already been considered in the context of SOH waveguides [23], and values higher than 3000 pm/V are envisaged in future polymer systems [36]. By using a material with ten times larger nonlinearity, an unprecedented high efficiency of η = 290 000% W^{-1}cm^{-2} could be obtained, or equivalently, 100 times smaller pump powers would lead to the same optical gain. Moreover, the damage threshold of single slot SOH waveguides having much smaller cross-sections is larger than 16 dBm for CW operation [37], suggesting that a pump power of 20 dBm will be below the damage threshold of the device.

It is worth noticing that two-photon absorption (TPA) does not limit the performance of the device. Indeed, even assuming that the entire optical field was concentrated in the 0.4 μm^2 silicon cross-section, 20 dBm of pump power correspond to an intensity I = 25 MW/cm^2. This value, combined with a TPA coefficient β_{TPA} = 1 cm/GW [35], corresponds to an absorption coefficient as low as $\beta_{TPA}I$ = 0.025 cm^{-1} (0.1 dB/cm). Free-carrier absorption (FCA) does not constitute a problem either, since it settles in at even higher powers than TPA [38]. Similarly, also third-order nonlinear effects due to the Kerr nonlinearity of silicon can be neglected, since TPA would otherwise be significant as well [39].

We further observe that the silicon dioxide substrate has a (bulk) propagation loss smaller than 2 dB/cm for wavelengths up to 3.6 μm [8, 40] and the silicon itself is transparent in an even larger spectral domain [8]. Also the roughness of the silicon waveguide might induce scattering losses [41], but values below 7 dB/cm have already been demonstrated in (even smaller) single and multiple slot waveguides [42, 43]. The different propagation loss mechanisms will decrease the performance of the device, but because of a gain of 14 dB/cm at 20 dBm pump power, this will not lead to any fundamental change in our discussion.

5. Conclusion

In the present work we propose a silicon waveguide concept suited for three-wave mixing. For the first time it is shown that the necessary phase-matching is possible in a silicon-organic hybrid (SOH) waveguide. This could be achieved by dispersion engineering. Our device has high conversion efficiency, is based on standard materials and technologies, and allows all-optical signal processing, mid-IR generation, and lowest-noise optical parametric amplification with small optical pump powers.

Appendix

A. Mode conversion

The modes involved in the nonlinear process described above can be excited by taking advantage of a mode converter as the one shown in Fig. 5, which was developed for this purpose. This mode converter acts differently for different wavelengths. At the wavelength of 1550 nm the fundamental (quasi-)TE-mode of the slotted waveguide is converted to the TE$_{40}$-mode of the double slot waveguide (power transmission coefficient $|S_{21}|^2$ = −2 dB), while at the wavelength of 3100 nm the fundamental mode TE$_{00}$ of the double slot waveguide is excited with $|S_{21}|^2$ = −0.7 dB. This mode converter can be used at the input as well as at the output of the double slot waveguide in order to operate only with the fundamental mode in all the remaining parts of the photonic circuit. The minimum feature size is 100 nm (size of waveguide tip), meaning that e-beam fabrication is not required, and standard 193 nm DUV technology is sufficient.

There are many other mode converter schemes that may be used in order to convert the pump and signal into the respective higher-order modes. Mode converters can for instance be built using the multimode interference (MMI) coupler from Ref [44], specially designed Bragg gratings, or holograms.

$$TE_{00} \rightarrow TE_{40} \ @ \ 1550 \ nm$$
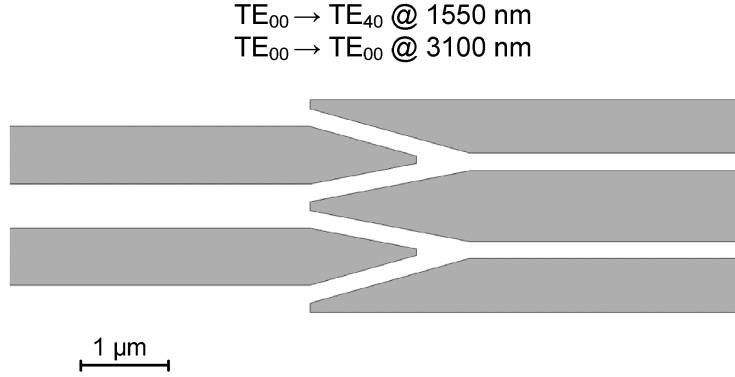$$TE_{00} \rightarrow TE_{00} \ @ \ 3100 \ nm$$

1 µm

Fig. 5. Slot to double slot mode converter. Light at wavelengths 1550 nm and 3100 nm is coupled in the slotted waveguide on the left. At the wavelength 1550 the fundamental mode of the slotted waveguide is converted into the TE_{40} mode of the double slot waveguide ($S_{21} = -2$ dB), while at the wavelength of 3100 nm the fundamental mode TE_{00} of the double slot waveguide is excited ($S_{21} = 0.7$ dB).

B. Third-order nonlinearity vs. second-order nonlinearity

For comparing third-order with second-order nonlinearity we calculate the electric field strength required for creating a certain polarization. The optical response of a material can be described by expanding the polarization $P(t)$ as a power series of the electric field strength $E(t)$. For simplicity we represent the vector fields P and E by scalar quantities,

$$P(t) = P^{(1)}(t) + P^{(2)}(t) + P^{(3)}(t) + \cdots, \qquad P^{(q)} = \chi^{(q)} E^q \qquad (13)$$

The second-order polarization $P^{(2)}$ is always larger than the third-order polarization $P^{(3)}$ if the electric field is smaller than the critical field

$$E_c = \frac{\chi^{(2)}}{\chi^{(3)}} \qquad (14)$$

If we now substitute $\chi^{(2)} = 230$ pm/V and $\chi^{(3)} = 10^5$ pm^2/V^2 (this value corresponds to the third-order nonlinear organic molecule DDMEBT [37, 45] which has previously been used for frequency conversion in SOI slot waveguides [37] and has one of the highest Kerr nonlinearities at 1.5 µm [46]), we find that the critical electric field is $E_c = 2.3 \ 10^9$V/m.

For the hypothetical case of a plane wave in vacuum, this field corresponds to an (enormous) intensity of $I = \varepsilon_0 \ c \ |E|^2 = 1.4 \ 10^{16}$W/m^2, or 140 W on an area of 100×100 nm^2. Since practical devices operate at intensities significantly smaller than the latter [9], $\chi^{(2)}$ waveguides will be more efficient than their $\chi^{(3)}$ counterparts.

Acknowledgments